http://dx.doi.org/10.5012/bkcs.2012.33.10.3368

Enhanced Gas Sensing Properties of Bi_2O_3-Core/In_2O_3-Shell Nanorod Gas Sensors

Sunghoon Park, Soyeon An, Hyunsung Ko, Changhyun Jin, and Chongmu Lee*

*Department of Materials Science and Engineering, Inha University, Incheon 402-751, Korea. *E-mail: cmlee@inha.ac.kr*
Received June 22, 2012, Accepted July 20, 2012

The Bi_2O_3 nanowires are highly sensitive to low concentrations of NO_2 in ambient air and are almost insensitive to most other common gases. However, it still remains a challenge to enhance their sensing performance and detection limit. This study examined the influence of the encapsulation of β-Bi_2O_3 nanorods with In_2O_3 on the NO_2 gas sensing properties. β-Bi_2O_3-core/In_2O_3-shell nanorods were fabricated by a two-step process comprising the thermal evaporation of Bi_2O_3 powders and sputter-deposition of In_2O_3. Multiple networked β-Bi_2O_3-core/In_2O_3-shell nanorod sensors showed the responses of 12-156% at 1-5 ppm NO_2 at 300 °C. These response values were 1.3-2.7 times larger than those of bare β-Bi_2O_3 nanorod sensors at 1-5 ppm NO_2. The enhancement in the response of β-Bi_2O_3 nanorods to NO_2 gas by the encapsulation by In_2O_3 can be accounted for based on the space-charge model.

Key Words : Bi_2O_3, In_2O_3, Nanorods, Sensor, NO_2

Introduction

Bithmuth oxide (Bi_2O_3) is an important wide band gap semiconductor material with four main crystallographic polymorphs denoted by α-, β-, γ-, and δ-Bi_2O_3.[1] Of these polymorphs, β-Bi_2O_3 is an n-type semiconductor, whereas δ-Bi_2O_3 is a p-type semiconductor. Due to its unique physical properties such as a large energy band gap, a high refractive index, a dielectric permittivity and a high oxygen conductivity, as well as remarkable photoconductivity and photoluminescence,[2-4] Bi_2O_3 has been extensively investigated for a range of applications in gas sensors, photovoltaic cells, optical coatings, fuel cells, supercapacitors, photocatalysts, *etc.*[1,5-7] Particularly regarding the gas sensor application, nanowires are expected to have significantly enhanced performance due to their ultrahigh surface-to-volume ratios and their dimensions comparable to Debye length,[8] which makes their electrical properties extremely sensitive to surface-adsorbed species. Bismuth oxide nanowires have been prepared using a range of techniques such as metal-organic chemical vapor deposition (MOCVD),[9] chemical methods,[10] and an oxidative metal vapor transport deposition technique,[11] a solution chemical method,[12] and a stress-induced method.[13] However, the vapor-liquid-solid (VLS) method has not been reported to synthesize Bi_2O_3 nanowires, yet. It is widely known that VLS process is the most successful for generating nanowires with single crystalline structures and in relatively large quantities among all vapor-based methods.[14]

The Bi_2O_3 nanowires are highly sensitive to low concentrations of NO_2 in ambient air and are almost insensitive to most other common gases.[12] However, it still remains a challenge to enhance their sensing performance and detection limit. Several techniques, such as surface functionalization,[15-17] doping[18-20] and heterostructure formation,[21-23] have been developed to enhance the sensing performance, detection limit and operation temperature of 1D nanostructure sensors. Among these techniques, the heterostructure formation method was used to enhance their sensing performance and detection limit further in this study. The β-Bi_2O_3-core/In_2O_3-shell nanorod sensors were fabricated and their NO_2 gas sensing properties were examined.

Experimental

The β-Bi_2O_3-core/In_2O_3-shell nanorods were synthesized using a two-step process: thermal evaporation of Bi powders in an oxidizing atmosphere and sputter-deposition of In_2O_3. First, Au-coated Si was used as a substrate for the synthesis of Bi_2O_3 nanostructures. Au was deposited on a (100) Si substrate by direct current (dc) magnetron sputtering. A quartz tube was mounted horizontally inside a tube furnace. 99.99% pure and bismuth (Bi) powders were placed on the lower holder at the center of the quartz tube. An Au-coated Si substrate was placed on the upper holder, approximately 5 mm apart from the source powders. The furnace was heated to 650 °C and maintained at that temperature for 1 h in a N_2/1 vol %-O_2 atmosphere with constant flow rates of oxygen (O_2) (3 sccm) and N_2 (300 sccm). The total pressure was set to 1 Torr. Subsequently, the as-synthesized Bi_2O_3 nanorods were coated with an In_2O_3 thin film using a radio frequency (RF) magnetron sputtering technique. The target used in this study was sintered stoichiometric In_2O_3. The sputtering was conducted in an Ar atmosphere (flow rate: 20 sccm). The vacuum chamber was evacuated to 1.0×10^{-6} Torr before introducing Ar. The substrate temperature, sputtering power, working pressure, and process time were 25 °C, 100 W, 2.0×10^{-2} Torr, and 15 min, respectively.

The morphology of the products was examined by field emission scanning electron microscopy (FESEM, Hitachi S-4200). The microstructures and compositions of the nanorod samples were characterized further by transmission electron

microscopy (TEM, Phillips CM-200) equipped with an energy dispersive X-ray spectrometer (EDXS). X-ray diffraction (XRD, Philips X'pert MRD) was performed using Cu-Kα radiation to identify the morphology and structure of the nanorod samples. For the sensing measurement, a SiO_2 film 300 nm thick was grown thermally on the single crystalline Si (100). Ni (~50 nm in thickness) and Au (~100 nm) thin films were deposited sequentially by sputtering to form electrodes the SiO_2-coated Si substrates using an interdigital electrode (IDE) mask. Multiple networked Bi_2O_3-core/In_2O_3-shell nanorods gas sensors were fabricated by pouring a few drops of nanorod-suspended ethanol onto oxidized Si substrates equipped with a pair of IDEs with a gap length of 20 μm. The electrical and gas sensing properties of the as-synthesized Bi_2O_3 nanorods and Bi_2O_3-core /In_2O_3-shell nanorods were determined at 300 °C in a quartz tube inserted in an electrical furnace. During the measurements, the nanorod gas sensors were placed in a sealed quartz tube with an electrical feed through. A given amount of NO_2 (> 99.99%) gas was injected into the testing tube through a microsyringe to obtain NO_2 concentrations of 1, 2, 3, 4, and 5 ppm while the electrical resistance of the nanorods was monitored. The response was defined as $(R_g-R_a)/R_a$ for NO_2 gas, where R_a and R_g are the electrical resistances of sensors in air and target gas, respectively. The response time was defined as the time required for the change in electrical resistance to reach 90% of the equilibrium value after injecting NO_2, and the recovery time was defined as the time needed for the sensor to return to 90% above the original resistance in air after removing the NO_2 gas.

Results and Discussion

Figure 1 shows a SEM image of the β-Bi_2O_3-core/In_2O_3-shell 1D nanostructures synthesized in this study. The nanorods ranged from 100 to 300 nm in diameter and from a few tens to a few hundreds of micrometers in length (Figure 1). An enlarged SEM image of a typical 1D nanostructure showed that it had a rod-like morphology (Inset in Figure 1). The EDX spectrum (Figure 2(a)) confirms that the core-shell

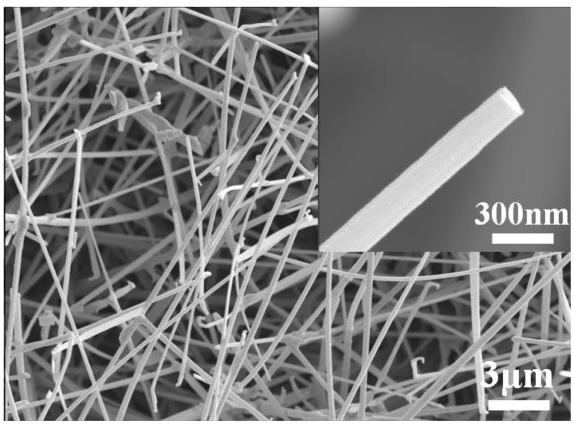

Figure 1. (a) SEM image of β-Bi_2O_3-core/In_2O_3-shell nanorods. Inset, the enlarged image of a typical core-shell nanorod.

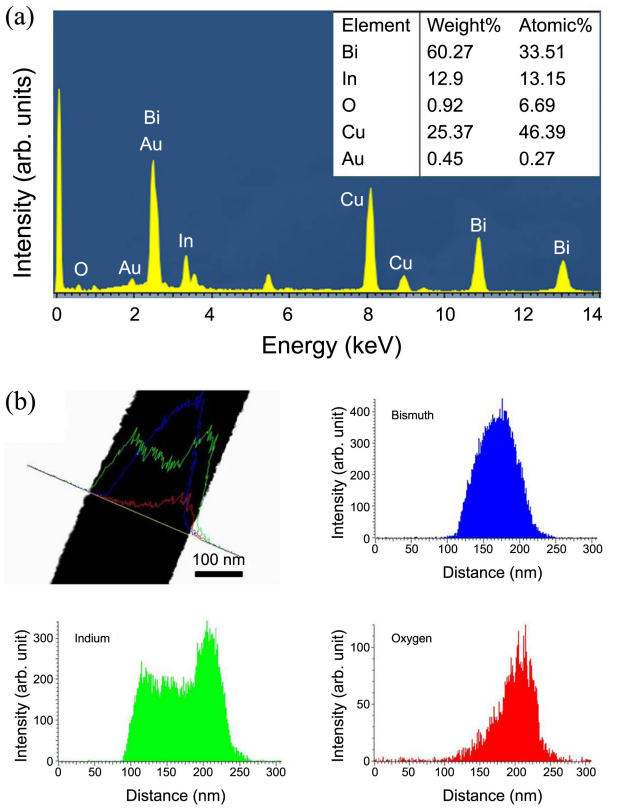

Figure 2. (a) EDX spectra of β-Bi_2O_3-core/In_2O_3-shell nanorods. (b) EDXS line scanning concentration profile across a line drawn perpendicular to the nanorod axis.

nanorod contained elemental Bi, In and O. The Au in the spectrum is due to the Au used as a catalyst for the VLS growth of the Bi nanorods. The Cu and C are due to the grid used for TEM sample preparation. On the other hand, figure 2(b) confirms that the core and shell of a core-shell nanorod consist of β-Bi_2O_3 and In_2O_3, respectively. The In detected in the central (core) region of the nanorod is due to the overlapping of the front and rear regions of the In_2O_3 shell with the Bi_2O_3 core from the viewpoint of the X-ray beam source used in the EDXS measurement.

Figure 3(a) shows a low-magnification TEM image of a typical as-synthesized core-shell nanorod, indicating that the thickness of the shell layer in the core-shell nanorod was approximately 8 nm. Figure 3(b) presents the local high-resolution TEM (HRTEM) image enlarging the core-shell interface area of the nanorod. The resolved spacings between the two neighboring parallel fringes in the core region corresponding to the tetragonal Bi_2O_3 (201) and (220) planes were approximately 0.32, and 0.27 nm, respectively. The corresponding selected area of the electron diffraction (SAED) pattern (Figure 3(c)), which was recorded perpendicular to the long axis, can be indexed for the $[\bar{1}12]$ zone axis of Bi_2O_3. The strong reflection spots in the corresponding selected area electron diffraction (SAED) pattern (Figure 3(c)) were assigned to the (201), (220), and (421) reflections of tetragonal-structured β-Bi_2O_3 with lattice constants, indicating that the β-Bi_2O_3 nanorod in the TEM image is a

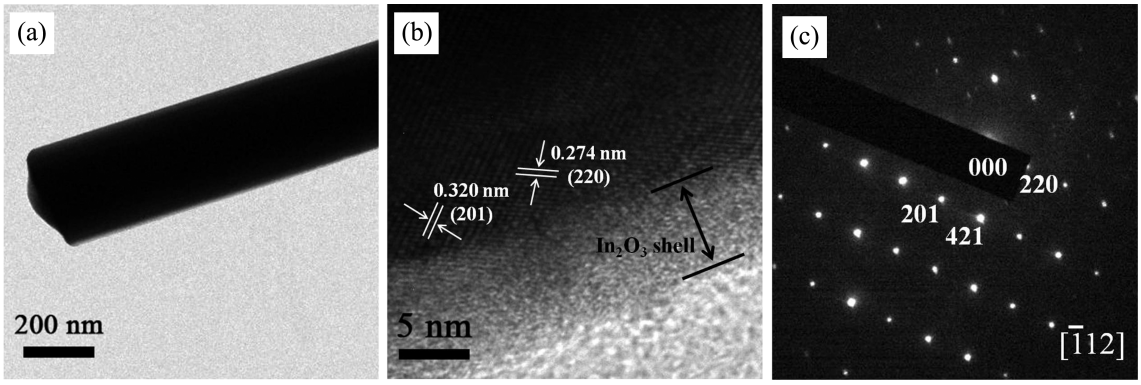

Figure 3. (a) Low-magnification TEM image of a typical β-Bi_2O_3-core/In_2O_3-shell nanorod. (b) Local HRTEM image of the nanostructure at the core-shell interface region. (c) SAED pattern of the [$\bar{1}$12] zone axis of the nanomaterial at the same region shown in the HRTEM image.

single crystal. Besides the strong reflections from the β-Bi_2O_3 core region, weak refection spots presumably from the In_2O_3 shell region were observed particularly on the upper side of the SAED pattern, indicating that the In_2O_3 shell region was crystalline locally even though crystallites were not clearly observed in the shell region in the SAED pattern. The HRTEM image and SAED pattern confirmed that the Bi_2O_3 core was a tetragonal-structured single crystal and that the In_2O_3 shell was mainly amorphous but locally crystalline.

Figure 4 shows the XRD patterns of the as-synthesized Bi_2O_3-core/In_2O_3-shell nanorods. The main reflection peaks in the pattern of the as-synthesized core-shell nanorods (Fig. 3(a)) can be indexed to a tetragonal structure, which is in good agreement with the reported data for bulk β-Bi_2O_3 crystals (JCPDS card No. 78-1793, a = 0.7741 nm, c = 0.5634 nm), indicating that the nanomaterial is Bi_2O_3. In addition, three reflection peaks indexed to a body-centered cubic structure, which is in good agreement with the reported data for bulk In_2O_3 crystals (JCPDS card No. 89-4595, a = 1.011 nm), were also observed in the pattern. The small number of reflection peaks with lower intensities implies that In_2O_3 shells are mostly amorphous but contain some nanocrystallites.

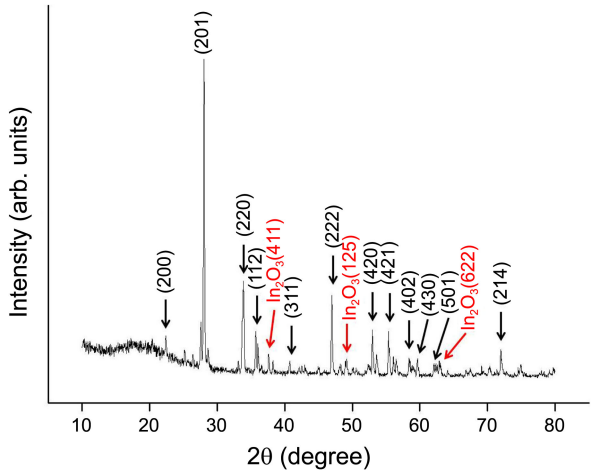

Figure 4. patterns of β-Bi_2O_3-core/In_2O_3-shell nanorods.

Figure 5(a) shows the dynamic responses of bare β-Bi_2O_3 nanorods and β-Bi_2O_3-core/In_2O_3-shell nanorods at 300 °C to a typical oxidizing gas NO_2. The resistance increased upon exposure to NO_2 and decreased even though it was not recovered completely to the initial value upon the removal of NO_2. Figures 5(b) and 5(c), respectively, show the enlarged part of the data in Figure 5(a) measured at a NO_2 concentration of 5 ppm for bare β-Bi_2O_3 nanorods (red line) and β-Bi_2O_3-core/In_2O_3-shell nanorods (black line) to reveal the moments of the gas input and gas stop. The bare β-Bi_2O_3 nanorods showed responses in a range of approximately 4-99% at the NO_2 concentrations of 1-5 ppm (Table 1). In contrast, the β-Bi_2O_3-core/In_2O_3-shell nanorods showed responses in a range of approximately 12-156% at the NO_2 concentrations of 1-5 ppm, respectively (Table 1). Therefore, the responses of the nanorods were improved by approximately 1.3-2.7 times at NO_2 concentrations of 1-5 ppm through the encapsulation of β-Bi_2O_3 nanorods with In_2O_3. Figure 5(d) shows that both the bare β-Bi_2O_3 nanorod sensor and the β-Bi_2O_3-core/In_2O_3-shell nanorod sensor tend to increase in response as the concentration of the NO_2 increases. This result agrees well with the general tendency that the response of a sensor increases with increasing the concentration of the target gas. The core-shell nanorods showed a higher increasing rate of the response with the NO_2 concentration than the bare β-Bi_2O_3 nanorod sensor.

The NO_2 gas sensing mechanism of the bare β-Bi_2O_3 nanorods can be depicted as follows: At this point, it is worthy of remembering that both β-Bi_2O_3 and In_2O_3 are n-type semiconductors. Upon exposure of the Bi_2O_3 nanorods to a strong oxidizing gas NO_2, NO_2 molecules are adsorbed by the Bi_2O_3 surface. The adsorption of NO_2 on the surface of the β-Bi_2O_3 nanorods results in an increase in resistivity, which can be explained by the following reactions:[24,25]

$$NO_2\,(g) + e^- \leftrightarrow NO_2^-\,(ads) \quad (1)$$

$$NO_2\,(g) + e^- \leftrightarrow NO\,(g) + O^-\,(ads) \quad (2)$$

Both these reactions take electrons from the conduction band of β-Bi_2O_3, resulting in an increase in resistivity.

On the other hand, the substantial improvement of the

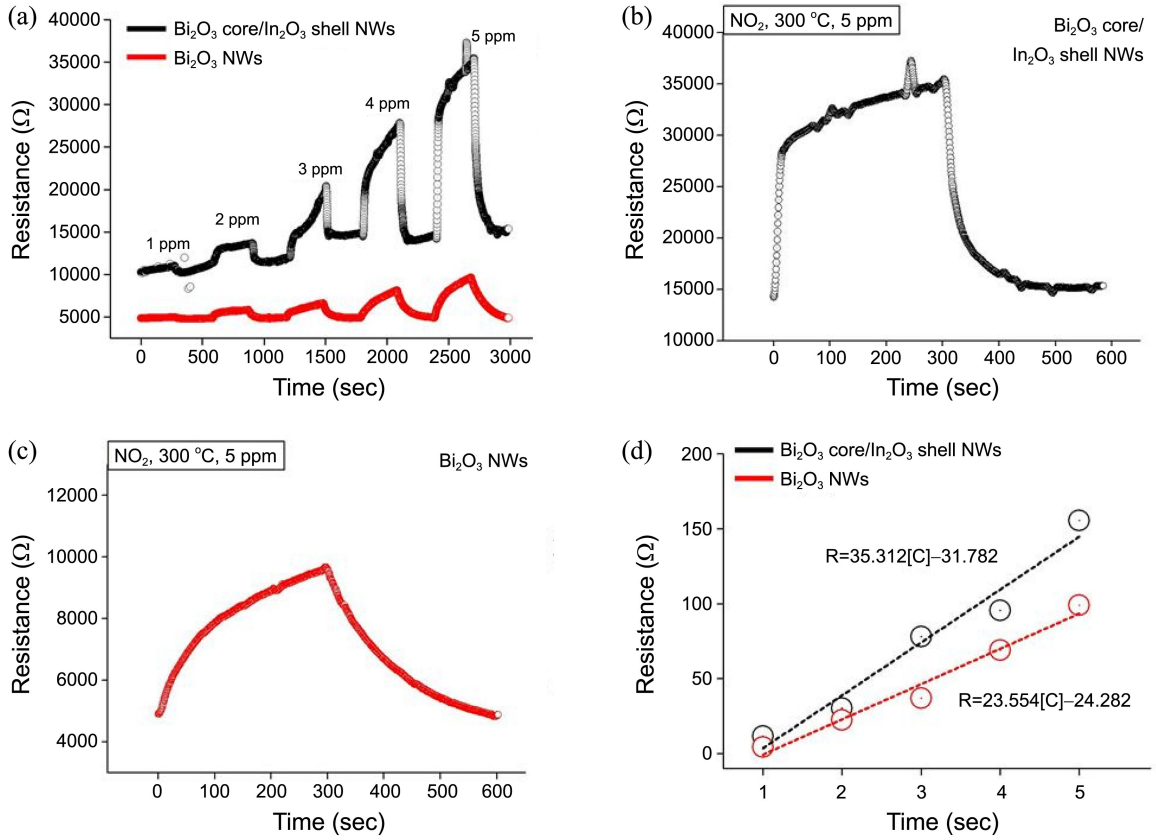

Figure 5. (a) Dynamic responses of the β-Bi_2O_3 nanorod and β-Bi_2O_3-core/In_2O_3-shell nanorod sensors. (b) Enlarged part of the β-Bi_2O_3-core/In_2O_3-shell nanorod sensor at 5 ppm NO_2 in (a). (c) Enlarged part of the β-Bi_2O_3 nanorod sensor at 5 ppm NO_2 in (a). (d) Responses of the β-Bi_2O_3 nanorod and β-Bi_2O_3-core/In_2O_3-shell nanorod sensors as a function of the NO_2 gas concentration.

response of the β-Bi_2O_3 nanorods to NO_2 gas by encapsulating them with In_2O_3 can be explained by the space-charge model.[26,27] NO_2 is a strong oxidizing gas. Upon exposure to NO_2 gas, the NO_2 gas is adsorbed by the core-shell nanorod sensor and electrons are released from the β-Bi_2O_3 shell layers, and attracted to the adsorbed NO_2 molecules because an oxidizing gas, such as NO_2 acts as an electron acceptor in the reaction. This reaction will result in an increase in the depletion layer width, and an increase in the resistance of the nanorod sensor. On the other hand, trapped electrons are released to the In_2O_3 shell layer by NO_2 gas after stopping the supply of NO_2 gas, leading to a decrease in the depletion layer width and resistance. The electron exchange between the surface states and the β-Bi_2O_3 shell layer occurs within the surface layer excluding the depletion layer. The width of the surface layer is the order of the Debye length λ_D which can be expressed as follows:[28,29]

$$\lambda_D = (\varepsilon kT/q^2 n_c)^{1/2} \quad (3)$$

where ε is the static dielectric constant (= 9.11 × 8.85 × 10^{-12} F/m in In_2O_3), k is the Boltzmann constant (= 1.38 × 10^{-23} joule/K), T is the absolute temperature (= 573 K), q is the electrical charge of the carrier (= 1.6 × 10^{-19} coulomb), and nc is the carrier concentration (= ~1.0 × 10^{17}/cm^3: the value obtained by Hall measurement for the In_2O_3 thin film prepared on the Si (100) substrate by sputtering). For the

Table 1. Relative responses measured at different NO_2 concentrations, for the bare β-Bi_2O_3 nanorod sensor and the β-Bi_2O_3-core/In_2O_3-shell nanorod sensor

NO_2 Conc.	Response (%)	
	Bi_2O_3	Bi_2O_3 core/In_2O_3 shell
1 ppm	4.39	11.65
2 ppm	22.57	30.09
3 ppm	36.91	78.03
4 ppm	68.97	95.49
5 ppm	98.91	155.51

In_2O_3 layer in the core-shell nanorods fabricated in this study, the λ_D value for 300 °C was calculated to be approximately 15.8 nm. This means that NO_2 molecules not only deplete the electrons in the In_2O_3 shell layer, the width of which is as small as approximately 8 nm, but also further take electrons from the β-Bi_2O_3 core. Therefore, in the β-Bi_2O_3-core/In_2O_3-shell nanorods, the heterojunction barrier existing at the interface of the core and shell should also be considered because electron transport is modulated by the heterojunction. The conductivity σ can be expressed as follows:[30]

$$\sigma = \sigma_0 \exp(-\Phi_{eff}/kT), \quad (4)$$

where σ_0 is a constant, Φ_{eff} the effective energy barrier at

the heterojunction, k a Boltzmann constant, T the absolute temperature. Upon exposure to NO_2 gas, Φ_{eff} will increase because NO_2 gas is adsorbed by the core-shell nanorod and electrons will be attracted to the adsorbed NO_2 molecules. Consequently, the conductivity of the core-shell nanorod will decrease or the resistivity will increase. On the other hand, after stopping the NO_2 gas supply, the electrons trapped by the adsorbed NO_2 molecules will be released and then trapped not only by the In_2O_3 shell layer but also by the β-Bi_2O_3 core *via* the heterojunction. Φ_{eff} will decrease because the trapped electrons will return to the conduction bands of β-Bi_2O_3 and In_2O_3. Consequently, the resistivity of the core-shell nanorod will will decrease. Therefore, electron transport is modulated by the heterojunction with an adjustable energy barrier height. In other words, the heterojunction acts as a lever in electron transfer by which the electron transfer is facilitated or restrained, resulting in enhanced sensing properties of the core-shell nanorod sensor.

Conclusions

β-Bi_2O_3-core/In_2O_3-shell nanorods were fabricated using a two-step process comprising thermal evaporation of Bi powders and sputter-deposition of In_2O_3. The nanorods were 100-300 nm in diameter and a few tens to a few hundreds of micrometers in length. The Bi_2O_3 core was found to be a tetragonal-structured single crystal and the In_2O_3 shell was mainly amorphous but locally crystalline. Multiple networked β-Bi_2O_3-core/In_2O_3-shell nanorod sensors showed responses in a range of 12-156% at 1-5 ppm NO_2 at 300 °C. These response values were 1.3-2.7 times larger than those of bare β-Bi_2O_3 nanorod sensors at 1-5 ppm NO_2. The enhancement in the response of the Bi_2O_3 nanorods to NO_2 gas by the encapsulation of them with In_2O_3 can be accounted for based on the space-charge model. The β-Bi_2O_3-In_2O_3 heterojunction acts as a lever in electron transfer by which electron transfer is facilitated or restrained, resulting in enhanced sensing properties of the core-shell nanorod sensor.

Acknowledgments. This study was supported financially by the Korean Research Foundation (KRF) through the 2010 Core Research Program.

References

1. Cabot, A.; Marsal, A.; Arbiol, J.; Morante, J. R. *Sens. Actuators B* **2004**, *99*, 74.
2. Fruth, V.; Popa, M.; Berger, D.; Ramer, R.; Gartner, M.; Ciulei, A.; Zaharescu, M. *J. Eur. Ceram. Soc.* **2005**, *25*, 2171.
3. Fan, H. T.; Teng, X. M.; Pan, S. S.; Ye, C.; Li, G. H.; Zhang, L. D. *Appl. Phys. Lett.* **2005**, *87*, 231916.
4. Thayer, R. L.; Randall, C. A.; Trolier-McKinstry, S. *J. Appl. Phys*. **2003**, *94*, 1941.
5. Sardar, K.; Fang, T.; Yang, T. W. *J. Am. Ceram. Soc.* **2007**, *90*, 4033.
6. Gujar, T. P.; Shinde, V. R.; Lokhande, C. D.; Han, S. H. *J. Power Sources* **2006**, *161*, 1479.
7. Zhou, L.; Wang, W.; Xu, H.; Sun, S.; Shang, M. *Chem. Eur. J.* **2009**, *15*, 1776.
8. Shen, G.; Chen, P.; Ryu, K.; Zhou, C. *J. Mater. Chem*. **2009**, *19*, 828.
9. Kim, H. W.; Myung, J. H.; Shim, S. H. *Solid State Commun*. **2006**, *137*, 196.
10. Gujar, T. P.; Shinde, V. R.; Lokhande, C. D.; Han, S. H. *Mater. Sci. Eng. B* **2006**, *133*, 177.
11. Qiu, Y.; Liu, D.; Yang, J.; Yang, S. *Adv. Mater*. **2006**, *8*, 2604.
12. Gou, X.; Li, R.; Wang, G.; Chen, Z.; Wexler, D. *Nanotechnol.* **2009**, *20*, 495501.
13. Park, Y. W.; Jung, H. J.; Yoon, S. G. *Sens. Actuators B* **2011**, *156*, 709.
14. Lu, Y.; Zhong, J. *Norwood*; Todd, S., Ed.; Artech House, Inc.: MA, 2004.
15. Gundiah, G.; Govindaraj, A.; Rao, C. N. R. *Chem. Phys. Lett*. **2002**, *351*, 189.
16. Zhang, H. Z.; Kong, Y. C.; Wang, Y. Z.; Du, X. Bai, Z. G.; Wang, J. J.; Yu, D. P.; Ding, Y.; Hang, Q. L.; Feng, S. Q. *Solid State Commun.* **1999**, *109*, 677.
17. Kim, B. C.; Sun, K. T.; Park, K. S.; Im, K. J.; Noh, T.; Sung, M. Y.; Kim, S.; Nahm, S.; Choi, Y. N.; Park, S. S. *Appl. Phys. Lett.* **2002**, *80*, 479.
18. Kim, H.; Park, S.; Jin, C.; Lee, C. *Nano: Brief Reports and Reviews* **2011**, *6*, 455.
19. Gao, Y. H.; Bando, Y.; Sato, T.; Zhang, Y. F.; Gao, X. Q. *Appl. Phys. Lett*. **2002**, *81*, 2267.
20. Tang, C. C.; Fan, S. S.; de la Chapelle, M. L.; Li, P. *Chem. Phys. Lett*. **2001**, *333*, 12.
21. Sanchez-Castillo, M. A.; Couto, C.; Kim, W. B.; Dumestic, J. A. *Angew. Chem*. **2004**, *116*, 1160.
22. Jágerszki, G.; Gyurcsányi, R. E.; Höfler, L.; Pretsch, E. *Nano Lett.* **2007**, *7*, 1609.
23. Oshima, Y.; Onga, A. *Phys. Rew. Lett*. **2003**, *91*, 205503.
24. Belysheva, T. V.; Bogovtseva, L. P.; Kazachkov, E. A.; Serebryakova, N. V. J. *Anal. Chem*. **2003**, *58*, 583.
25. Ferro, R.; Rodriguez, J. A.; Bertrand, P. *Thin Solid Films* **2008**, *516*, 2225.
26. Xu, C.; Tamaki, J.; Miura, N.; Yamazoe, N. *Sens. Actuators B* **1991**, *3*, 147.
27. Zhu, C. L.; Chen, Y. J.; Wang, R. X.; Wang, L. J.; Cao, M. S.; Shi, X. L. *Sens. Actuators B* **2009**, *140*, 185.
28. Ogawa, H.; Nishikawa, M.; Abe, A. *J. Appl. Phys.* **1982**, *53*, 4448.
29. Barsan, N.; Weimar, U. *J. Electroceram*. **2001**, *7*, 143.
30. Weis, T.; Lipperheide, R.; Wille, U.; Brehme, S. *J. Appl. Phys.* **2002**, *92*, 1411.